

Obtention, Characterization and Deposition of Hydroxyapatite Obtained from Scales of the Amazonian Fish Pirarucu (*Arapaima gigas*) Using the High Velocity Suspension Plasma Spray (HVSPS) Process

Érico Drummond Dantas Silveira^{a*} , Jean Carlos Silva Andrade^a , Reinaldo de Almeida Rodrigues^b ,
Cláudia Cândida Silva^b , Felipe de Souza Miranda^c , José Costa de Macedo Neto^b 

^aUniversidade Federal do Amazonas (UFAM), Programa de Pósgraduação em Ciência e Engenharia de Materiais (PPGCEM), Manaus, AM, Brasil.

^bUniversidade do Estado do Amazonas (UEA), Escola Superior de Tecnologia, Departamento de Engenharia de Materiais, Manaus, AM, Brasil.

^cInstituto Tecnológico da Aeronáutica (ITA), Laboratório de Plasmas e Processos (LPP), São José dos Campos, SP, Brasil.

Received: September 06, 2022; Revised: January 08, 2023; Accepted: May 30, 2023

In this study, a hydroxyapatite (HA) coating derived from the scales of the Amazonian fish pirarucu (*Arapaima gigas*) was produced using calcination at 500 and 750 °C and deposited on AISI 316 stainless steel substrate using the process of thermal spraying, high velocity suspension plasma spray (HVSPS). To verify its potential, this material was characterized by X-ray diffraction (XRD), by which characteristic peaks of hydroxyapatite were evidenced. Via X-ray fluorescence (XRF) of the samples, it was observed that the Ca/P ratio was equal to 2.00. Using the Fourier transform infrared (FTIR) spectroscopy and Raman spectroscopy, it was possible to observe the characteristic bands of the HA. For the coating, the mechanical nanoindentation test showed mean Vickers microhardness (VH) values of 93.25 VH for the hydroxyapatite and of 196.57 HV for the substrate. The modulus of elasticity (EIT) was 77.85 GPa for the hydroxyapatite coating and 136.45 GPa for the substrate. Optical microscopy showed that the coating was homogeneously deposited.

Keywords: Hydroxyapatite, Calcination, Plasma spray coating, Bioceramics.

1. Introduction

The improvement of the properties of metal surfaces, such as their chemical stability, surface finish, roughness and interaction with the living organism are of great interest to the medical and dental industry and is being studied¹. As well as surface coating techniques, such as thermal spraying (TS), the use of hydroxyapatite ($\text{Ca}_{10}(\text{PO}_4)_6(\text{OH})_2$) has been investigated as a deposition material for the processing of metal alloys to be used as prostheses or implants in the human body, which despite having biocompatibility characteristics, do not promote the process of cell differentiation^{1,2}.

In recent studies, the need to control and slow down the degradation of biocompatible alloys such as magnesium-based alloys, which today are used as an alternative to titanium alloys, can be achieved through the use of surface coatings with hydroxyapatite^{1,3,4}. The hydroxyapatite coating can also improve the biocompatibility of metal implants and increase the osteoblastic response, thus promoting osseointegration. In addition, it can also control the degradation of magnesium, thus providing an environment conducive to the regeneration of bone tissue^{3,4}.

To obtain HA, other methods of synthesis can be used, either by a natural agent or by a synthetic one. Via a natural agent: calcination; alkaline hydrolysis; sol-gel precipitation;

mechanical chemical; microwave irradiation; chemical precipitation; ultrasonic irradiation. Via a synthetic agent: dry methods (solid state and mechanical); wet methods (chemical precipitation, hydrolysis, sol-gel, hydrothermal, emulsion and sonochemical) and high temperature processes (combustion and pyrolysis)^{5,6}.

Given the importance of the use of hydroxyapatite coatings in metal alloys in order to improve biocompatibility in the human body, in this study, hydroxyapatite was obtained from a natural, sustainable and lower-cost agent than synthetic hydroxyapatite. The success of the biocompatibility process is due to the deposition of hydroxyapatite on the substrate. In this work, a high-speed deposition process was used that provides rapid deposition with water as an economical and abundant precursor liquid, since this allows the removal of impurities and does not modify the hydroxyapatite.

In this study, the hydroxyapatite coating was derived from the scales of the Amazonian pirarucu fish (*Arapaima gigas*) since, in the preparation of this fish for consumption, its scales are discarded and have no further use. The hydroxyapatite obtained in this work was deposited by the high velocity suspension plasma spray process on AISI 316 stainless steel. This process uses a dynamic plasma thermal spray sample port, which generates a supersonic plasma jet with an axial injection that provides heat transfer between

*e-mail: drummondeds@gmail.com

plasma and particle up to 200% greater than conventional ones. The spray used promoted a deposition layer without changing the HA crystallinity and thus avoided the use of other heat treatments after spraying. The presence of characteristic phases, elemental chemical composition of the hydroxyapatite obtained by calcination of the fish scales at 500 °C and 750 °C. Finally, after the characterizations by XRD (*used to characterize the scale structures in their natural form and the calcined samples in order to verify the structural behavior of crystallinity and the presence of hydroxyapatite and other possible phases of apatite*), FTIR (*used to complement the characterization by XRD, through the wavelength of the vibrational bands, which are characteristic of the functional groups with calcium; phosphate and hydroxyl of the hydroxyapatite molecule*), XRF (*used to verify the Ca/P ratio of the samples obtained*), digital optical microscopy (*used to characterize of the sprayed layers*) and nanoindentation (*used to verify the microhardness and modulus of elasticity, and the mechanical characteristics of the material before spraying and after spraying*), it was possible to further develop the material.

2. Materials and Methods

2.1. Synthesis of HA powder from pirarucu scales

For the obtention of the hydroxyapatite samples, the scales were acquired at the Manaus Moderna Municipal Market, which is located in the center of Manaus, Amazonas state, Brazil. These were removed from leftover pieces of pirarucu packaged. After collection, the fish scales went through four stages, to create the hydroxyapatite. In Step 1: the scales were separated then cleaned to remove impurities for the next step. Step 2: the scales were washed with running water without adding any chemicals. Then the scales were dried at room temperature, ready for the next stage, which is heat treatment by calcination. The scale has a dark part (external) and a lighter part (internal). Images of Pirarucu and Pirarucu scales can be found in the Supplementary material (Figure S1). Step 3: the scales were exposed to a calcination heat treatment at two different temperatures: 500 °C and 750 °C, obtaining two samples. The scales exposed to calcination at 500°C were inserted into the muffle-type electric furnace at room temperature, with a heating rate of 10°C per minute. After reaching a temperature of 500°C, the sample remained for another 8 hours. The scales exposed to calcination at 750°C were inserted into the muffle-type electric furnace at room temperature, with a heating rate of 10°C per minute. After reaching a temperature of 750°C, the sample remained for another 8 hours. For both samples, the cooling rate was 10°C per minute, inside the muffle itself, until reaching room temperature. Step 4: after removing the scales from the muffle furnace, already calcined, they were manually ground with the aid of pistil and mortar, then sieved until reaching the desired grain size, which was measured using a 425 mm/μm sieve (ABNT/ASTM 40 and TYLER/MESH 35). The result was the obtainment of two samples: the sample calcined at 500 °C with a grayish appearance, and the sample at 750 °C with a whitish appearance. The samples were then characterized.

2.2. Substrate preparation

The substrate used was AISI 316 stainless steel with dimensions of 20 mm x 10 mm, which was cut on a bench band saw and finished by milling. Eight samples simultaneously were used in the processes. The plasma itself also cleans the substrate during the preheating step of the material, which is the step before the deposition process. The substrate was then cleaned with acetone⁷. *Acetone cleaning can be considered standard and plasma cleaning to improve the surface cleaning quality of stainless steel.*

2.3. Characterization

The characterization of the samples obtained allowed us to evaluate the structure and presence of *the calcium phosphate phase obtained*, as well as the Ca/P ratio, the elements present, its mechanical resistance, the thickness of the deposited layer and the functional groups in the hydroxyapatite molecule. For this, the following techniques were used:

X-ray fluorescence. The fluorescence technique was used to verify the Ca/P ratio of the samples obtained, since there are several phases for apatites⁸. The analyses were performed in wave dispersion X-ray fluorescence (WD-XRF) equipment, (Supermini, Rigaku, USA) with a palladium tube, exposure time of 200 s and power of 200 W. The analytical crystals LIF 200, PET and RX25 were used. For each sample, with the aid of a 10,000 Kgf press, fine powder tablets with uniform granulometry were prepared, whose composition presented 1,000 g of the sample, which was homogenized with 4,000 g of high purity H₃BO₃ in agate mortar.

X-ray diffraction: XRD was used to characterize the scale structures in their natural form and the calcined samples at 500 °C and 750 °C in order to verify the structural behavior of crystallinity and the presence of hydroxyapatite and other possible phases of apatite. The characterization was performed using XRD equipment (Empyrean, Malvern Panalytical, UK). with a step size of 0.02°, 2θ interval of 15° a 60° and step time of 0.6 s. The results were compared with standard cards for the apatite phases found in the Joint Committee for Powder Diffraction Studies database (JCPDS) file number 09-0432 for hydroxyapatite.

Fourier Transform Infrared Spectroscopy (FTIR): This was used to complement the characterization by XRD, through the wavelength of the vibrational bands, which are characteristic of the functional groups with calcium; phosphate and hydroxyl of the hydroxyapatite molecule. The infrared vibrational characteristics of the samples were obtained using a spectrometer (PerkinElmer Frontier, PerkinElmer, USA) in ATR mode, with 32 accumulations, in the range of 4000 to 400 cm⁻¹, resolution 4 cm⁻¹, gain 1.

RAMAN spectroscopy: This was used as a characterization technique capable of verifying the presence of organic and inorganic materials through the analysis of vibration and rotation of molecules, both of the structure and chemical nature of the materials. Raman spectra were collected using a Raman microscope (Evolution, Horiba, Kyoto, Japan) with excitation wavelength in the visible spectrum (532 nm).

Characterization by digital optical microscopy: The images of the surface of the stainless steel substrate, AISI316L,

before spraying with the hydroxyapatite sample, and after the coating is applied to the substrate (magnified from 20X and 40X), were obtained using a digital microscope (VHX-100, Keyence, Mexico). The images of the cross section of the sprayed layers, the were obtained the magnified from 200X and 1000X. To obtain the images of the deposited layers and measure the thickness, the samples were polished using a polishing equipment (Aropol 1V, Arotec, Brazil), silk cloth for polishing (Durplan, Ø 200mm, Brazil) and diamond paste (1 µm, Solotest, Brazil).

XRD characterization of the sprayed layer: The technique used to characterize the layer deposited by the plasma process was XRD using a diffractometer (X²pert Powder, Panalytical, UK), with a step size of 0.02°, 2θ interval of 15° a 100° and step time of 10 s. This analysis aimed to verify possible changes in the characteristics of the HA present in the samples obtained and previously characterized before spraying.

Nanoindentation: The nanoindentation test was performed with hardness testing equipment (HM 2000, Fischerscope, Germany) according to ASTM E384-17⁹ and ASTM E2546-15¹⁰ standards. The load used was 1000 mN for 5 s in order to verify the microhardness and modulus of elasticity, and the mechanical characteristics of the material before spraying and after spraying.

2.4. Sample application in plasma spray (HVSPS)

For the application in the processing and deposition by high velocity suspension plasma spray process, the sample used was obtained from calcination at 750 °C, since this was the temperature with the least organic influence on the scale and so that the spray torch was not contaminated. The powder was prepared in a dispersing solution based on distilled water at a ratio of 500 mL of water to 5 g of the sample obtained. The substrate used was AISI 316 stainless steel. The application time was 5 min after heating, in five samples of the base material. Images of the scheme of HVSPS System can be found in the supplementary material (Figure S2).

High velocity suspension plasma spray process features: 90 mm application distance from plasma torch nozzle; samples are rotated at 80 min⁻¹; N₂ gas flow rate of 270 L/min; precursor liquid flow rate of 80 mL/min; a dynamic sample holder with a three-dimensional (3D) position and rotation control with the ability to process eight samples simultaneously is used. The operating parameters of the plasma torch were fixed at the current and voltage of 100 A and 340 V, respectively; it is necessary to preheat for 2 minutes at 200 °C before starting the deposition process⁷. Images of the application of the sample in the plasma spray images can be found in the supplementary material (Figure S3).

3. Results and Discussion

3.1. X-ray fluorescence

The Ca/P ratio of the samples obtained at 500 °C and 750 °C was equal to 2.00, which is characteristic of the tetracalcium phosphate phase (TTCP) of the chemical formula Ca₄O(PO₄)₂⁸, was identified in samples calcined at both temperatures. A Ca/P ratio of around 2.00 has been previously observed in studies of synthesis of hydroxyapatite derived from natural agents such as fish scales and mammalian bones¹¹⁻¹⁴. Numerous impurities, such as fluorine, magnesium, sodium, potassium, carbonate and chloride, can be found in bones, as well as small amounts of elements such as strontium, barium, copper, zinc and iron, which are commonly associated with biological apatite and can be seen as substituents in the structure of apatite¹².

3.2. X-ray diffraction

In Table 1, the characteristic reflections of the samples obtained by calcination of the scale at 500 °C, calcination of the scale at 750 °C, and of the scale in its natural state were compared with Joint Committee for Powder Diffraction Studies (JCPDS) card number 09-0432 for hydroxyapatite. Characteristic reflections of hydroxyapatite were observed in all diffraction patterns of all samples.

The diffractogram of the sample obtained from the scale calcined at 500 °C showed characteristic reflections of hydroxyapatite at the Bragg angle of 2θ = 31.8° (Table 1) (Figure 1). It is also possible to observe an increase in the number of diffraction reflections when compared with the XRD of the scale in its natural state. The diffractogram of the sample obtained from the scale calcined at 750 °C showed the presence of the crystalline hydroxyapatite phase, with more reflections when compared with the XRD of the sample calcined at 500 °C, and with the same reflections when compared with the JCPDS card 09-0432 (Figure 1). Previous studies of the characterization by XRD of samples obtained from the calcination of fish scales and bones in order to obtain HA show the same characteristic peak of greater intensity at the angle 2θ = 31.8°, with [211] being the main diffraction plane^{14,15}.

Differences in crystallinity can be attributed to differences in the concentrations of minor constituents, for example, Mg, N, CO₃, HPO₄, a fact that may be associated with the organic fraction and are composed mainly of collagen, connective tissue proteins, water and other types of proteins present in the sample in its natural state^{11,15}. Identified and compatible with the results of X-ray fluorescence. The diffractogram of the sample obtained from the scales calcined at 750 °C was the one that presented a diffraction pattern closer to the standard JCPDS file 09-0432. A higher degree of crystallization of

Table 1. Characteristic reflections, hydroxyapatite (JCPDS 09-0432), *in natura* and samples calcined at 500 °C and 750 °C.

Sample	Angle 2 Theta (degrees)							
HA JCPDS	26.1	31.8	33.0	34.0	39.8	46.8	48.0	49.5
<i>IN NATURA</i>	26.1	31.8			39.7	46.8		
HA 500°C	26.1	31.8			39.7	46.8		49.5
HA 750°C	26.1	31.8	33.0	34.0	39.8	46.8	48.0	49.5

the sample was confirmed due to the intensity of the sharp reflection and the well-resolved reflections in the diffractograms of higher calcination temperatures^{14,15}.

3.3. Fourier Transform Infrared Spectroscopy (FTIR)

The FTIR spectra of the sample obtained from the scales calcined at 500 °C and 750 °C show the characteristic modes of absorption, in the interval bands of 4000–400 cm⁻¹ (Figure 2), of the phosphate (PO₄⁻³) and hydroxyl (OH) functional groups, which are characteristic of hydroxyapatite, as well as the presence of the carbonate group (CO₃⁻²)^{14,16-18}. The first indication of the formation of HA is present in the bands between 1,000–1,100 cm⁻¹, which is associated with the vibration mode of asymmetric elongation for the P-O group¹⁹.

The symmetric stretch mode, $\nu_1(\text{PO}_4^{-3})$ centered at 961 cm⁻¹, the two intense bands found at 1031 cm⁻¹ and 564 cm⁻¹, related to anti-symmetric stretch $\nu_3(\text{PO}_4^{-3})$ and anti-symmetric deformation $\nu_4(\text{PO}_4^{-3})$, respectively, in the

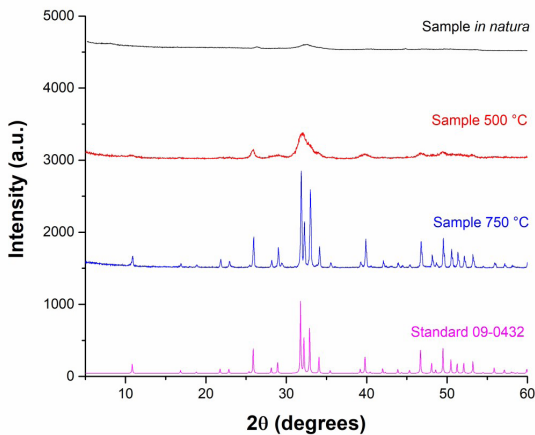


Figure 1. Diffractogram of the scale *in natura* and when calcined at 500 °C and 750 °C compared with the standard hydroxyapatite.

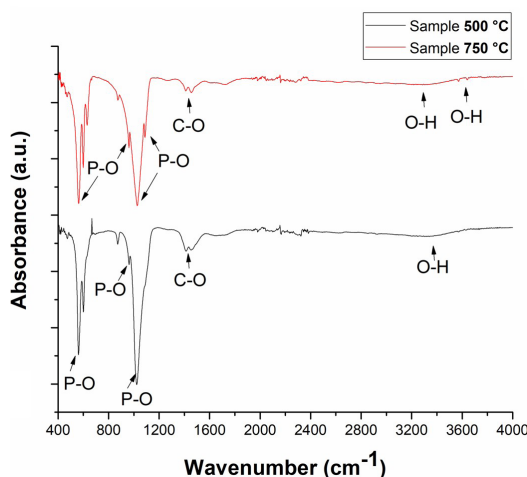


Figure 2. Sample calcined at 500 °C and 750 °C and deposited by high velocity suspension plasma spray process. Range: 4000–400 cm⁻¹.

bands between 1200 and 400 cm⁻¹ indicate a crystallized HA¹⁶⁻¹⁹. In addition, between 1200 and 400 cm⁻¹, it is also possible to identify the presence of the symmetric deformation mode $\nu_2(\text{CO}_3^{-2})$ centered at 873 cm⁻¹. This behavior was due to the interaction of carbon dioxide with the samples¹⁷⁻²⁰. Note both of these occur for the sample obtained from the scales calcined at 500 °C and for the sample obtained from the scales calcined at 750 °C (Figure 3). With regard to the oscillation mode of the hydroxyl ions, $\nu_L(\text{OH}^-)$, it is observed that with the increase in the calcination temperature of the scales from 500 °C to 750 °C, an increase in intensity arises around 631 cm⁻¹. This increase is related to the appearance of OH⁻ ions and is expected for the formation of the crystalline HA phase, as well as the components of the anti-symmetric deformation mode $\nu(\text{PO}_4^{-3})$ at 601 and 564, between the bands 750 to 500 cm⁻¹, which tend to become more intense and narrower as the structure becomes more crystalline (Figure 3)^{19,21}.

Around 3641 and 3571 cm⁻¹ are the vibrations corresponding to the hydroxyl stretch modes, $\nu_1(\text{OH}^-)$ (Figure 4), as well as the increase in intensity at 631 cm⁻¹ (Figure 3) for the oscillation mode of hydroxyl ions, $\nu_L(\text{OH}^-)$, which is associated with the increase in the calcination temperature of the scales from 500 to 750 °C, indicating the crystalline phase of hydroxyapatite¹⁹⁻²¹.

The region located between 1600–1200 cm⁻¹ (Figure 2), is possible to observe bands that correspond to the impurities of CO carbonate ions, which are characteristic of type A carbonate hydroxyapatite, and occupy hydroxyl sites around 1454 cm⁻¹, and of type B, around 1415 cm⁻¹ that occupy phosphate sites¹⁸⁻²². With the increase in the calcination temperature of the scales from 500 to 750 °C, it is observed that the intensity of the carbonate peaks of type A and type B in the region between 1600–1200 cm⁻¹ present a decrease in the scale sample calcined at 750 °C, due to the time that the sample remained at a high temperature^{19,21}. The reduction of the intensity with the increase of the calcination temperature of the scales is associated with the elimination of these impurities, thus making the material more crystalline (Figure 4).

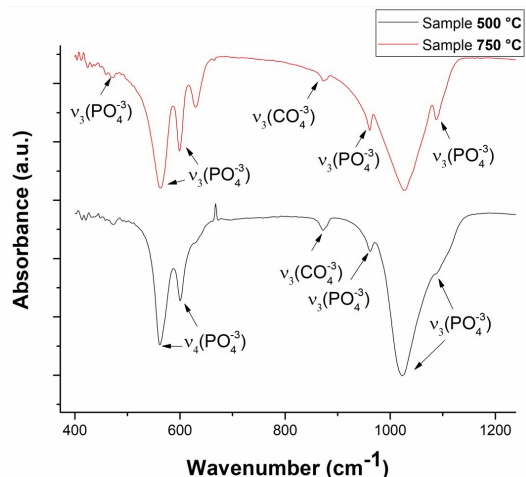


Figure 3. Sample calcined at 500 °C and 750 °C and deposited by high velocity suspension plasma spray process. Range: 1200–400 cm⁻¹.

Table 2. FTIR of the groups.

Groups	Hydroxyapatite	Carbonated HA	Sample 750 °C	Sample 500 °C
OH ⁻	3578		3571	
$\nu_1(\text{OH}^-)$			3641	
H ₂ O	1630	1630	1610	1641
$\nu_3(\text{CO}_3^{2-})$		1469		
$\nu_3(\text{CO}_3^{2-})$	1460	1454	1454	1454
$\nu_3(\text{CO}_3^{2-})$	1419	1415	1415	1415
$\nu_3(\text{PO}_3^{-4})$	1088	1090	1090	1090
$\nu_3(\text{PO}_3^{-4})$	1065	1060		
$\nu_3(\text{PO}_3^{-4})$	1035	1032	1031	1031
$\nu_1(\text{PO}_3^{-4})$	962	961	961	961
$\nu_2(\text{CO}_3^{2-})$	875	873	873	873
OH ⁻	631	634	631	631
$\nu_4(\text{PO}_3^{-4})$	602	605	601	601
$\nu_4(\text{PO}_3^{-4})$	574	575		
$\nu_4(\text{PO}_3^{-4})$	565	568	564	564

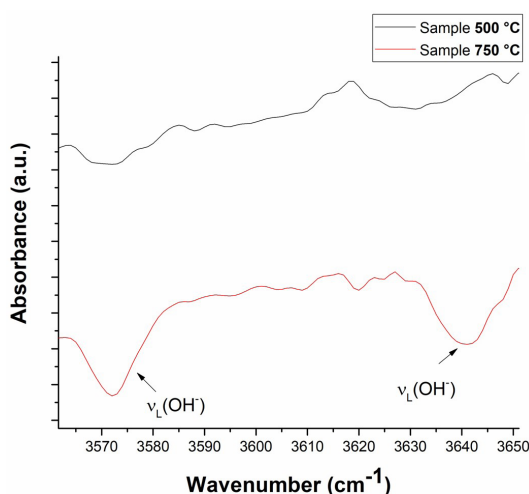
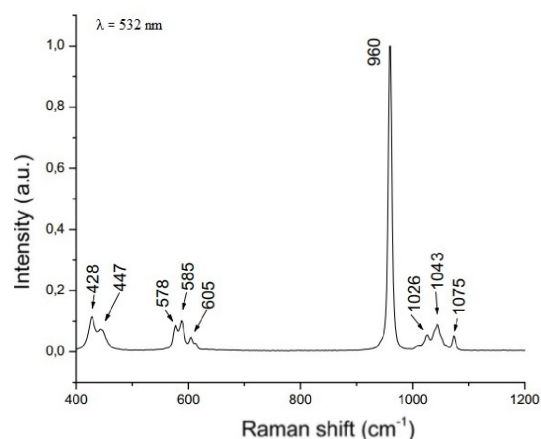
**Figure 4.** Sample calcined at 500 °C and 750 °C and deposited by high velocity suspension plasma spray process. Range: 3700-3500 cm⁻¹.

Table 2 was elaborated with data from the FTIR bands characteristic of the vibrational modes of HA, based on the literature cited in this study, compared to the bands found in the scale sample calcined at 500 °C and the scale sample calcined at 750 °C^{16-19,21}.

3.4. RAMAN spectroscopy

Figure 5 shows only the Raman spectrum of the scale sample calcined at 750 °C since this characterization cannot be applied to the scale sample calcined at 500 °C due to the strong presence of organic matter. An intense band at 960 cm⁻¹ is attributed to the symmetrical stretch mode of the phosphate group $\nu_1(\text{PO}_4^{-3})$ that is characteristic of HA^{16,19,23-25} (Figure 5). In addition, vibration bands found

**Figure 5.** Raman spectroscopy of the sample calcined at 750 °C.

at 1026 cm⁻¹, 1043 cm⁻¹ and 1075 cm⁻¹ correspond to the antisymmetric stretch of $\nu_3(\text{PO}_4^{-3})$ associated with the P–O bond. Centered peaks of the O–P–O bonds are observed at 578 cm⁻¹, 585 cm⁻¹ and 605 cm⁻¹ and attributed to the antisymmetric $\nu_4(\text{PO}_4^{-3})$ vibrations. Modes associated to the O–P–O bonds at 428 cm⁻¹ and 447 cm⁻¹ are associated with the deformation mode $\nu_2(\text{PO}_4^{-3})$, which clearly indicate the presence of the hydroxyapatite phase in the sample^{19,23-25}.

As with the results of FTIR, it was possible to observe the presence of CO₃ ions occupying phosphate sites (type B) at 1075 cm⁻¹, evidencing the carbonated hydroxyapatite²³⁻²⁵. The carbonate that occupies the sites of functional groups of hydroxyapatite is considered to be an impurity of the mineral, and is thus associated with the presence of the organic fraction due to the collagen present in the pirarucu scale^{21,23,24}. It can also change the crystallinity of hydroxyapatite as well as the occupied dimensions, and has a limited range for the

presence of carbonate in the molecular structure without breaking the crystal¹¹.

3.5. Characterization by digital optical microscopy

It is possible to observe the difference on the surface of the stainless steel substrate, AISI316L, before spraying with the hydroxyapatite sample, Figure 6A, and after the coating is applied to the substrate, Figure 6B, which is fixed to the holder - dynamic sample.

Imperfections with micro-cavities on the substrate surface, Figure 7(A), are indicated by the dots in a). This result was expected, as the substrate did not undergo any preparation prior to spraying. From the analysis of the surface with coating applied to the substrate, Figure 7B, a microstructure of the two zones shown by a) and b) can appear, which is common in plasma spray, and which shows the numerous agglomerates that are similar to the “cauliflower” zone a), which results in a high concentration of the raw material of the suspension and of the powder that did not have the necessary preparation, such as adequate refinement, as well

as areas without agglomerates in b)^{19,23}. The suspension was axially injected into the spray torch with a continuous flow, resulting in the fragmentation of droplets, which when they come into contact with the plasma torch, quickly atomize and evaporate the solvent (vehicle) of the suspension.

The cross section, magnified by 200X, was obtained by the digital microscope, shows thermal spray coatings of the scale sample calcined at 750 °C, which are relatively dense with some microporosity marked in a) (Figure 8A). The sample appears to exhibit cone-like tips marked in b), which are typical of coatings sprayed with raw material from precursor suspension, with its thickness estimated at 60µm by digital optical microscopy¹⁹. The cross section, magnified 1000X, corroborates with the evidence of the previous image, since it reveals the characteristic deposits obtained from a highly concentrated suspension showing the agglomerated particles composed of cracks marked “b”, and particles with microspores in “a” (Figure 8B). The morphology of the particles found, are associated with the process used in this study, which uses a suspension where the solid part already exists and the liquid only carries the particle that when fused and accelerated settles on the substrate⁷.

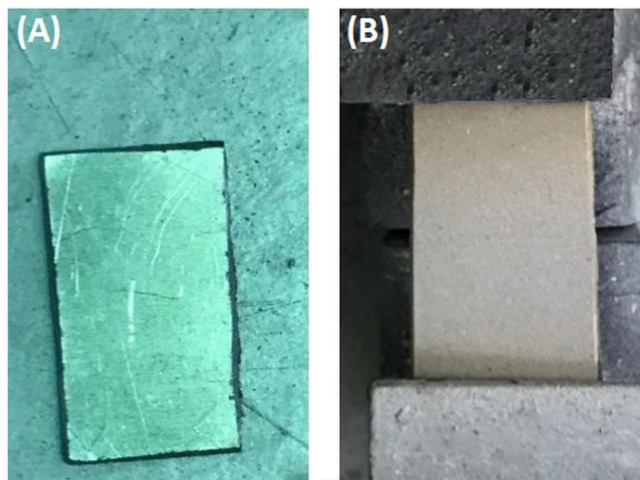


Figure 6. Substrate (AISI 316L stainless steel) without sprayed layer (A) and with sprayed layer (B).

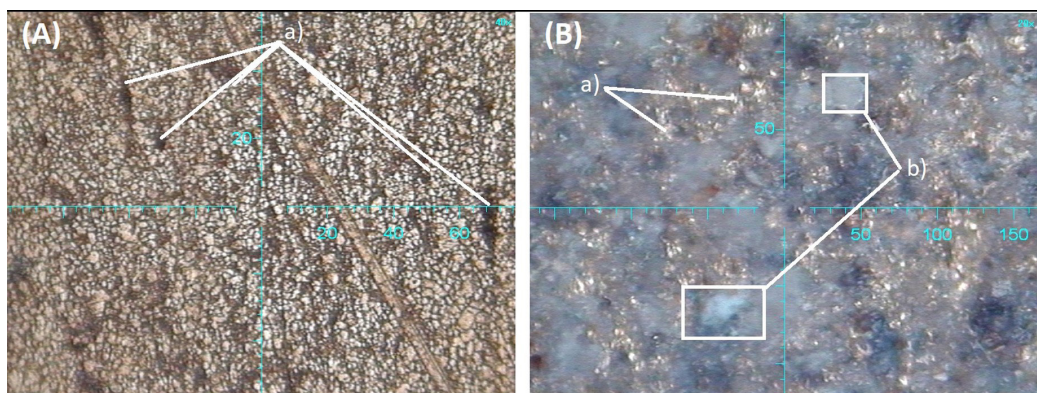


Figure 7. Substrate surface with deposition and amplified 40X (A) and amplified 20X (B).

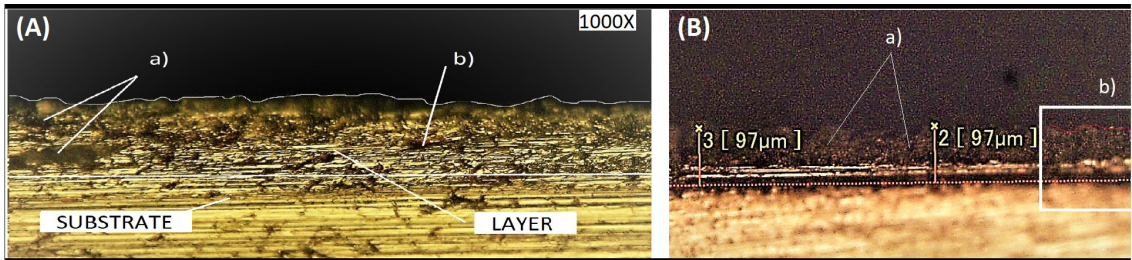


Figure 8. Sprayed layer. Amplified 1000X (A). Sprayed layer with estimated thickness. Amplified 200X (B).

3.6. XRD characterization of the sprayed layer

The diffraction pattern performed after thermal spraying (sprayed layer) presented for the sprayed sample, a crystalline structure with peaks, $2\theta = 31.8^\circ$ of great intensity, 33° , 49.5° , 46.8° , 34° , 39.8° and 48° , characteristic of HA, with the main diffraction plane [211], (Figure 9). This result differs from the results obtained in the study by²⁶, in which the authors found structures of amorphous coatings; however, such a result was already expected by the author who used long distances and low-energy plasma for the deposition of the raw material.

The maintenance of the crystallinity of the sprayed sample may be related to the passage of the sample through the plasma at high temperature, which reaches around 6000°C though with rapid cooling, and which also collaborates with the elimination of impurities associated with the presence of carbonate ions in the sample, thus avoiding other phases of hydroxyapatite¹⁹

The properties and performance of the hydroxyapatite deposition used in the plasma spray process are closely related to its manufacturing process. The coatings and their formation mechanism are associated with the different variables of the process, and the crystallinity of the deposition alone does not induce the quality of the coating due to the appearance of various forms of hydroxyapatite, such as forms that are unfused, recrystallized and have an absence of hydroxyls. Control in the process of thermal spraying was of fundamental importance for a good result¹⁶.

3.7. Nanoindentation

For the mechanical nanoindentation test, two sample alloy AISI 316L was studied one with and other without the hydroxyapatite coating. Was utilized five indentations with the load used was 1000 mN for a period of 5 s. The maximum indenter penetration depth for the alloy with the hydroxyapatite coating was $9.712\ \mu\text{m}$ and, for the uncoated substrate, it was $4.699\ \mu\text{m}$. The depth of penetration was greater in the coated substrate since, in a larger penetration area, there is a greater possibility of interactions between the indenter and a wide variety of deep cracks, pores and other defects found in the deposited layer (Figure 10), which has a wide variety of random local spatial orientation²⁷. The mean and standard deviation Vickers microhardness (VH) and modulus of elasticity (EIT) values were $93.25\ \text{VH} \pm 67.22$ and $77.85\ \text{GPa} \pm 42.53$ for the hydroxyapatite-coated substrate, respectively, and $196.57\ \text{VH} \pm 21.64$ and $136.45\ \text{GPa} \pm 10.83$ for the uncoated substrate, respectively. This reduction in microhardness and modulus

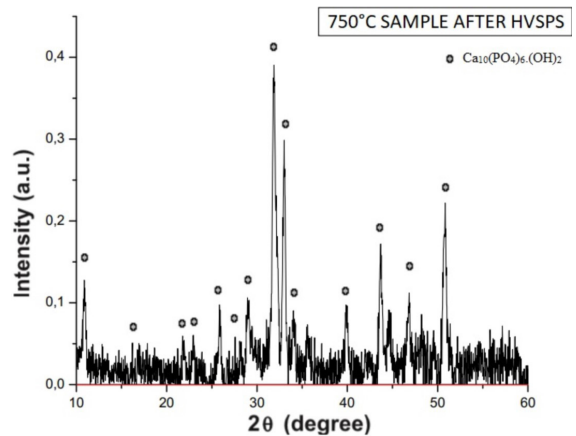


Figure 9. Diffraction pattern of the coating of the obtained layer.

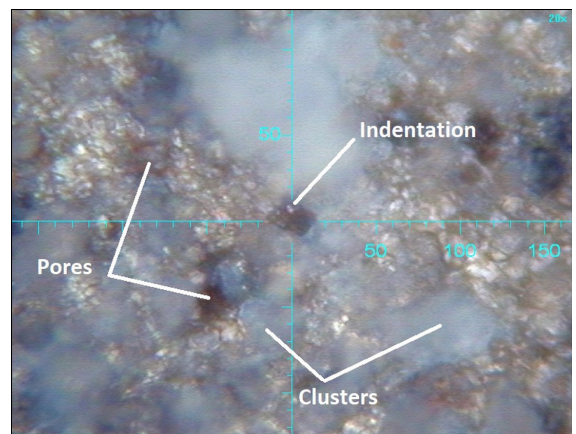


Figure 10. Indentation of the HA coating with pores and clusters.

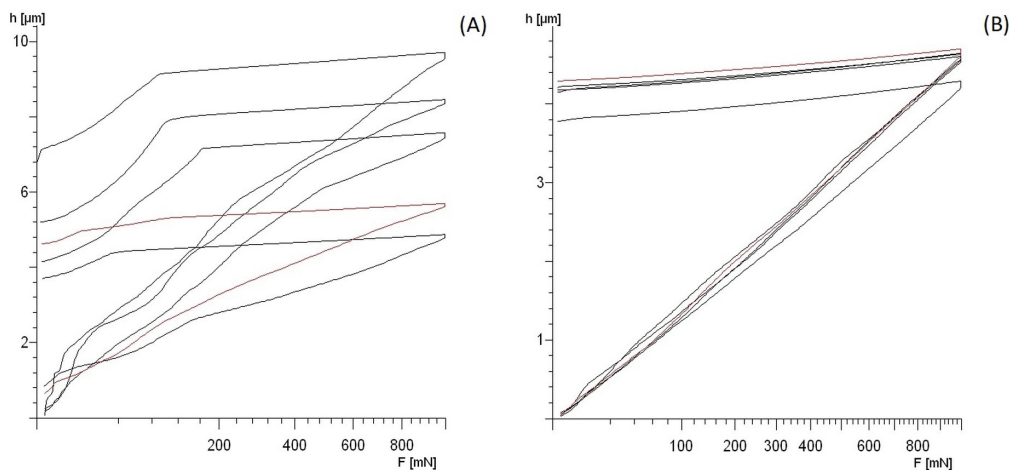
of elasticity of the substrate with hydroxyapatite coating in relation to the uncoated substrate may be associated with the difference in the thickness of the layers, since the ceramic characteristic of the hydroxyapatite layer resists indentation less than the metal surface of the alloy used⁴. Anova analyzes were performed for the average microhardness and elastic modulus between the samples with and without hydroxyapatite coating (Tables 3 and 4). From Table 3 it is observed that the $F < F_{\text{critic}}$ values. This means that the mean Vickers microhardness values do not show significant differences.

Table 3. Test results for microhardness.

Source of variation	Sum of squares	Degrees of freedom	Mean square	F	P-value	F critic
Between samples	16012.530	1	16012.530	6.422	0.064	7.708

Table 4. Test results for modulus of elasticity.

Source of variation	Sum of squares	Degrees of freedom	Mean square	F	P-value	F critic
Between samples	5162.670	1	5162.660	5.355	0.081	7.708

**Figure 11.** Load displacement of the coating of the obtained sample (A). Load displacement of the substrate (B).

From Table 4, it is observed that the $F < F_{critic}$ values. This means that the mean values of the modulus of elasticity do not show significant differences.

The difference in linearity in the initial phase of nanoindentation that is present in the loads between 0 mN and 200 mN, Figure 11A, is due to the deposition layer of the hydroxyapatite sample. When compared with the linearity in the same range from 0 mN to 200 mN, Figure 11B, of the nanoindentation applied directly to the metal substrate, the presence of different contact surfaces found by the indenter can be confirmed. This difference between surfaces contributes to the divergent values when the deposited material has higher hardness than the substrate⁴, in the same way as the modulus of elasticity and hardness values, and similar to that found in this study for the materials deposited with hydroxyapatite^{27,28}. The minimum, 4,868 μm and the maximum, 9,712 μm indentation depth of the coating obtained in sample (Figure 10) corresponded to approximately 6 and 12%, respectively, of the estimated thickness of the HA layer, which was obtained from the calcination of the scale at 750 °C (60 μm , by optical microscopy).

4. Conclusions

In this study, the HA was obtained from the scales of the pirarucu fish using calcination at 500 °C and 750 °C. To confirm the acquisition of hydroxyapatite, the samples were characterized and the results obtained by XRF gave

the ratio $\text{Ca/P} = 2$, which indicated tetracalcium phosphate apatite (TTCP) for the samples with calcination temperatures at 500 °C and 750 °C. The sample obtained by calcination at 750 °C presented a crystalline structure of hydroxyapatite that was comparable to the JCPDS card number 09-0432 for hydroxyapatite. The characterization by FTIR showed the presence of carbonate – CO_3^- ions occupying sites of hydroxyl groups (type A) and phosphate sites (type B) in the region of 1600-1300 cm^{-1} , thus suggesting HA carbonate for the samples with calcination at 500 °C and at 750 °C. After spraying, in the plasma spray process (HVSPS), via XRD, it was observed that the crystallinity of the hydroxyapatite was maintained. There was also the elimination of the tricalcium phosphate phase (TCP- β), previously observed before the spraying process.

In the mechanical characterization by nanodentation, the maximum penetration depth of the indenter for the alloy with the coating was 9,712 μm and for the uncoated substrate, it was 4,699 μm , which suggests penetration of the sample with the deposited layer. The mean Vickers microhardness (VH) and modulus of elasticity (EIT) values were 93.25 VH and 77.85 GPa for the substrate with the hydroxyapatite coating, respectively, and 96.57 VH and 136.45 GPa for the uncoated substrate, respectively. For samples with calcination at 500 °C and 750 °C, the minimum and maximum indentation depths corresponded to approximately 6 and 12%, respectively, of the estimated 60 μm thickness layer by optical microscopy.

5. References

- Miranda G, Sousa F, Costa MM, Bartolome F, Silva FS, Carvalho O. Surface design using laser technology for Ti6Al4V-hydroxyapatite implants. *Opt Laser Technol.* 2008;109:488-95.
- Ratha I, Datta P, Balla VK, Nandi SK, Kundu B. Effect of doping in hydroxyapatite as coating material on biomedical implants by plasma spraying method: a review. *Ceram Int.* 2020;47:4426-45.
- Iskandar ME, Aslani A, Liu H. The effects of nanostructured hydroxyapatite coating on the biodegradation and cytocompatibility of magnesium implants. *J Biomed Mater Res.* 2013;101A:2340-54.
- Surmeneva MA, Surmenev RA. Microstructure characterization and corrosion behaviour of a nano-hydroxyapatite coating deposited on AZ31 magnesium alloy using radio frequency magnetron sputtering. *Vacuum.* 2015;117:60-2.
- Lewis G. Nanostructured hydroxyapatite coating on bioalloy substrates: current status and future directions. *J Adv. Nanomater.* 2017;2:65-82.
- Mohd Pu'ad NAS, Koshy P, Abdullah HZ, Idris MI, Lee TC. Syntheses of hydroxyapatite from natural sources. *Heliyon.* 2019;5:1-14.
- Miranda FS, Caliani FR, Campos TM, Essiptchouk AM, Filho GP. Deposition of graded SiO₂ / SiC coatings using high-velocity solution plasma spray. *Ceram Int.* 2017;43:16416-23.
- Costa ACFM, Lima MG, Lima LHMA, Cordeiro VV, Viana KMS. Hidroxiapatita: obtenção, caracterização e aplicações. *REMAP.* 2009;3:29-39.
- ASTM: American Society for Testing and Materials. ASTM E384-17: standard test method for microindentation hardness of materials. West Conshohocken: ASTM; 2017.
- ASTM: American Society for Testing and Materials. ASTM E2546-15: standard practice for instrumented indentation testing. West Conshohocken: ASTM; 2015.
- LeGeros RZ, Ben-Nissan B. Introduction to synthetic and biologic apatites. *Adv Calcium Phosphate Biomater.* 2014;28:17-28.
- Boyd AR, Rutledge L, Randolph LD, Meenan BJ. Strontium-substituted hydroxyapatite coatings deposited via a co-deposition sputter technique. *Mater Sci Eng C.* 2015;46:290-300.
- Pon-on W, Suntornsaratoon P, Charoenphandhu N, Thongbunchoo J. Hydroxyapatite from fish scale for potential use as bone scaffold or regenerative material. *Mater Sci Eng C.* 2016;62:183-9.
- Sun R, Lv Y, Niu Y, Zhao X, Cao D, Tang J, et al. Physicochemical and biological properties of bovine-derived porous hydroxyapatite/collagen composite and its hydroxyapatite powders. *Ceram Int.* 2017;43:16792-8.
- Panda NN, Pramanik K, Sukla LB. Extraction and characterization of biocompatible hydroxyapatite from fresh water fish scales for tissue engineering scaffold. *Bioprocess Biosyst Eng.* 2014;37:433-40.
- Xu H, Geng X, Liu G, Xiao J, Li D, Zhang Y. Deposition, nanostructure and phase composition of suspension plasma-sprayed hydroxyapatite coatings. *Ceram Int.* 2016;42:1-7.
- Mondal B, Mondal S, Mondal A, Mandal N. Fish scale derived hydroxyapatite scaffold for bone tissue engineering. *Mater Charact.* 2016;121:112-24.
- Candidato RT Jr, Paw L, Lecomte-nana G, Constantinescu C, Denoirjean A. Development of hydroxyapatite coatings by solution precursor plasma spray process and their microstructural characterization. *Surf Coat Tech.* 2017;318:39-49.
- Candidato RT Jr, Sergi R, Jouin J, Noguera O, Paw L. Advanced microstructural study of solution precursor plasma sprayed Zn doped 60 hydroxyapatite coating. *J Eur Ceram Soc.* 2018;38:2134-44.
- Bulina NV, Chaikina MV, Yu I, Prosanov IY, Dudina DV. Strontium and silicate co-substituted hydroxyapatite: mechanochemical synthesis and structural characterization. *Mater Sci Eng B.* 2020;262:114719. <http://dx.doi.org/10.1016/j.mseb.2020.114719>.
- Hosseinzadeh E, Davarpanah M, Nemati NH, Tavakoli SA. Fabrication of a hard tissue replacement using natural hydroxyapatite derived from bovine bones by thermal decomposition method. *Int J Organ Transplant Med.* 2014;5:23-31.
- Souza TS, Rangel FC, Tokumoto MS, Lôbo IP, Cruz RS. Síntese, caracterização e modificação da hidroxiapatita com zinco para aplicação na reação de esterificação. *Materia (Rio J).* 2019;24:1-8.
- Aruna ST, Kulkarni S, Chakraborty M, Kumar SS, Balaji N. A comparative study on the synthesis and properties of suspension and solution precursor plasma sprayed hydroxyapatite coatings. *Ceram Int.* 2017;43:9715-22.
- Unabia RB, Bonebeau S, Candidato RT Jr, Jouin J, Noguera O, Pawłowski L. Investigation on the structural and microstructural properties of copper-doped hydroxyapatite coatings deposited using solution precursor plasma spraying. *J Eur Ceram Soc.* 2019;39:4255-63.
- Nosenko VV, Yaremko AM, Dzhagan VM, Vorona IP, Romanyuk YA, Zatovsky IV. Nature of some features in Raman spectra of hydroxyapatite-containing materials. *J Raman Spectrosc.* 2016;47(6):726-30. <http://dx.doi.org/10.1002/jrs.4883>.
- Cañas E, Orts MJ, Boccaccini AR, Sánchez E. Solution precursor plasma spraying (SPPS): a novel and simple process to obtain bioactive glass coatings. *Mater Lett.* 2018;223:19-202.
- Dey A, Mukhopadhyay AK, Gangadharan S, Sinha MK, Basu D, Bandyopadhyay NR. Nanoindentation study of microplasma sprayed hydroxyapatite coating. *Ceram Int.* 2009;35:2295-304.
- Karimzadeh A, Ayatollahi MR, Bushroa AR, Herliansyah MK. Effect of sintering temperature on mechanical and tribological properties of hydroxyapatite measured by nanoindentation and nanoscratch experiments. *Ceram Int.* 2014;40:9159-66.

Supplementary material

The following online material is available for this article:

Figure S1 - (a) Pirarucu scales. (b) Scales after cleaning showing the inner white part and outer black part of the scale (Photo credits: Author, 2021).

Figure S2 - Scheme of HVSPS System: (1) tandem type plasma torch, (2) pressurized vessel, (3) needle valve, (4) solution flowmeter, (5) dynamic sample holder, (6) control and data acquisition system, (7) exhaust system and (8) atomizer nozzle [9].

Figure S3 - Application of the sample in the plasma spray. (Photo credit: Author, 2021).